Energy & Environmental Science

Accepted Manuscript

This article can be cited before page numbers have been issued, to do this please use: Z. Chen, X. Gao, L. Shan, Q. Fu, Z. Xing, P. Rao, Z. Kang, X. Shi, W. Zhang and X. Tian, *Energy Environ. Sci.*, 2025, DOI: 10.1039/D5EE02763B.

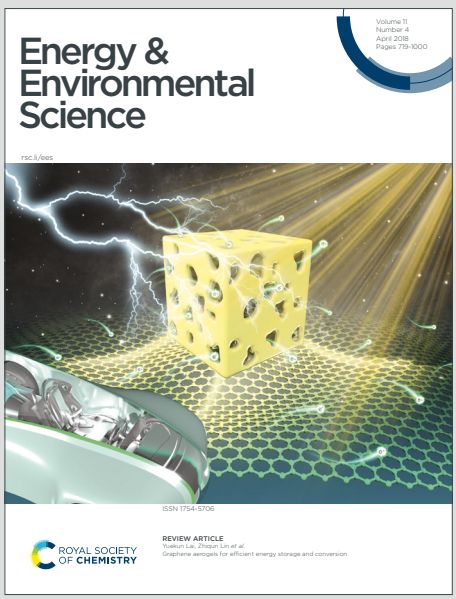

ROYAL SOCIETY OF CHEMISTRY

rsc.li/ees

Broader context

Zinc-iodine battery is regarded as promising candidate for energy storage device, while the practical application is still blocked by severe polyiodide shuttle effect, leading to active iodine loss, Zn corrosion, and rapid capacity decay. Resorcinol (RSC), with benzene ring and phenolic hydroxyl groups, is demonstrated as an effective electrolyte additive to stabilize both the iodine-loading cathode and Zn anode. The theoretical calculations and experimental data manifest that RSC molecules hold strong chemisorption capability for polyiodides and strengthened iodine conversion reaction kinetics. As expected, zinc-iodine batteries in RSC-containing electrolyte exhibit high-capacity retention rate of 85.8% after 10000 cycles at 1 A g^{-1}, as well as 90.1% after 17000 cycles at 5 A g^{-1}. In addition, the corresponding pouch batteries with high-iodine loading of 12.7 mg cm^{-2} deliver a high reversible capacity of 165.8 mA h g^{-1} after 200 cycles at 0.5 A g^{-1}. This work proposes a practical electrolyte modification strategy to guarantee durable zinc-iodine batteries.

Taming polyiodides: Phenol chemistry for shuttle-free and durable zinc-iodine batteries

Zhixiang Chen [a,#], Xinlei Gao [a,#], Lutong Shan [b,#], Qingjin Fu [d], Zhenyue Xing [a], Peng Rao [a], Zhenyu Kang [a], Xiaodong Shi [a,*] , Wei Zhang [c,*], and Xinlong Tian [a,*]

[a] School of Chemistry and Chemical Engineering, School of Marine Science and Engineering, State Key Laboratory of Tropic Ocean Engineering Materials and Materials Evaluation, Hainan University, Haikou, 570228, China

[b] Department of Chemistry, University of Manchester, Manchester, M139PL, UK.

[c] Christopher Ingold Laboratory, Department of Chemistry, University College London, London, WC1H0AJ, UK.

[d] Tsinghua Shenzhen International Graduate School, Tsinghua University, Shenzhen, 518055, China

* Corresponding authors emails: shixiaodong@hainanu.edu.cn; wei.zhang.21@ucl.ac.uk; tianxl@hainanu.edu.cn

[#] These authors contributed equally.

Abstract

Zinc-iodine ($Zn-I_2$) batteries have emerged as promising candidates for large-scale energy storage, but the practical application is still significantly hindered by the notorious polyiodide shuttle effect, which always results in active iodine loss, severe zinc corrosion, and irreversible capacity attenuation. Herein, resorcinol (RSC), constructed by benzene ring and phenolic hydroxyl groups, is verified as an effective electrolyte additive to simultaneously stabilize the iodine-loading cathode and zinc anode of $Zn-I_2$ batteries. Theoretical calculations demonstrate RSC molecules hold more negative adsorption energies for polyiodides and lower Gibbs free energies for iodine reduction process, manifesting strong chemisorption capability for polyiodides and strengthened iodine conversion kinetics. Consequently, $Zn||AC@I_2$ batteries in RSC-containing electrolyte deliver high reversible capacity of 141.1 mA h g^{-1} and high retention rate of 85.8% after 10000 cycles at 1 A g^{-1}. Even after 17000 cycles at 5 A g^{-1}, the reversible capacity stabilizes at 106.2 mA h g^{-1} with high retention rate of 90.1%. The corresponding pouch batteries with high iodine loading of 12.7 mg cm^{-2} present high capacity of 165.8 mA h g^{-1} and high retention rate of 97.9% after 200 cycles at 0.5 A g^{-1}. This work provides a cost-effective strategy to inhibit polyiodide shuttle behavior, and ensure durable cyclic stability of $Zn-I_2$ batteries.

Keywords: Zinc-iodine batteries; Resorcinol additive; Chemisorption interaction; Polyiodide shuttle effect; Durable cyclic stability

1. Introduction

Lithium-ion batteries have been widely applied in electric vehicles and portable electronics due to the high energy density. However, high cost, safety concerns, and limited resource availability necessitate the exploration of alternative battery chemistries[1, 2]. Among them, zinc-iodine (Zn-I_2) batteries, have emerged as promising candidates due to high safety, low cost, and environmental friendliness[3-5]. Zn-I_2 batteries, which use iodine as the cathode material, benefit from the relative abundance of iodide in seawater, high capacity of 211 mA h g^{-1}, and suitable voltage platform of 1.3 V[6-8]. These features make Zn-I_2 batteries particularly attractive for grid energy storage system. However, despite their promise, the practical commercialization of Zn-I_2 batteries is significantly blocked by several fundamental challenges, primarily the shuttle effect of polyiodide intermediates[9-11].

The polyiodide shuttle originates from the iodine-loading cathode with high concentration polyiodides, which migrate through separator and reach zinc anode during cycling process [12]. These polyiodides will uncontrollably react with metallic zinc ($Zn + I_x^- \rightarrow Zn^{2+} + xI^-$), leading to direct zinc corrosion and low zinc utilization rate[13, 14]. Meanwhile, the resulting self-discharge behavior of Zn-I_2 batteries brings poor cycling stability and low capacity retention[6, 15]. Besides, the interface side reactions on the Zn anode also induce the formation of alkaline by-products and Zn-I clusters[16, 17], which are difficult to diffuse back to the cathode, causing severe capacity decay[18]. Therefore, addressing polyiodide shuttle of iodine-loading cathode and interface instability of Zn anode becomes the central focus to improve electrochemical performance of Zn-I_2 batteries. Many strategies have been proposed to tackle these issues. For instance, carbonaceous host materials were used to adsorb iodine species and inhibit the polyiodide shuttle effect[19, 20]. Unfortunately, the physical adsorption between carbon materials and iodine species was too weak to prevent the shuttle effect over extended cycling period[21-23]. High concentration electrolytes and gel electrolytes were adopted to suppress active iodine dissolution and the formation of polyiodides[24-26]. Though these electrolytes mitigated the shuttle effect to some extent, their high viscosity impeded the diffusion of Zn^{2+} ions and reduced the reaction kinetics.

Additionally, constructing protective layers on the surface of Zn anode, such as zeolite[27], and zinc silicate[28], was effective to block parasitic reaction and promote uniform zinc deposition. Nonetheless, these artificial interface layers often require complex fabrication process, and achieving reliable and uniform coatings in large scale remains challenging[14, 29]. Thus, it is an imperious demand for a facile and cost-effective strategy to simultaneously prevent polyiodide shuttle and interface side reactions.

In this work, resorcinol (RSC), consisting of a benzene ring and two phenolic hydroxyl groups, is demonstrated as an effective and functional electrolyte additive to break the deadlock of Zn-I_2 batteries. Theoretical calculations demonstrate RSC molecules hold stronger binding energies for iodine species and lower Gibbs free energies for iodine conversion reactions, restraining the polyiodides accumulation on iodine-loading cathode and the parasitic corrosion reactions on Zn anode. Meanwhile, the introduction of RSC effectively reduces the number of solvated H_2O molecules around Zn^{2+} ion, thereby alleviating the formation of interface by-products. Compared with the 2 M $ZnSO_4$ electrolyte (ZSO electrolyte), the Zn||AC@I_2 batteries in 2 M $ZnSO_4$ + 12 mM RSC composite electrolyte (RSC electrolyte) achieve high reversible capacity of 141.1 and 106.2 mA h g^{-1} after 10000 and 17000 cycles at 1 and 5 A g^{-1}, corresponding to high-capacity retention rate of 85.8% and 90.1%, respectively. Even for Zn||AC@I_2 pouch batteries, high iodine loading cathode (12.7 mg cm^{-2}) also displays high specific capacity of 165.8 mA h g^{-1} after 200 cycles at 0.5 A g^{-1} with high-capacity retention rate of 97.9%. This work offers valuable insight for the functional electrolyte design and facilitates the practical application of Zn-I_2 batteries.

2. Results and discussion

Fig. 1a schematically depicts the inherent advantages of phenol chemistry strategy on the iodine-loading cathode and zinc metal anode of Zn-I_2 batteries, which effectively inhibits the polyiodides accumulation and polyiodide shuttle behavior, mitigates the parasitic zinc corrosion, and facilitates the iodine conversion reaction kinetics. To verify this inference, ultraviolet-visible (UV-vis) absorption spectra were collected for the RSC-containing solution during the I_3^- adsorption process. Over time, the absorbance intensity of I_3^-

species in the mixed solution rapidly decreased, accompanied by a visible color change in the cuvette from yellow to colorless (**Fig. 1b**), indicating the strong chemisorption and capture capability of RSC for polyiodides. Similarly, the UV-vis absorption spectra of RSC-containing solution during I_2 adsorption process are also collected. As presented in **Figs. 1c, S1a**, the absorbance intensity of I_2 species in the solution continuously decreases, while the absorbance intensity of I_3^- species initially increases and then decreases, further suggesting the positive role of RSC in promoting chemical conversion and chemisorption for iodine species. Eventually, the solution color in the cuvette turns colorless, which is not found in ZSO solution (**Figs. S1b, c**). **Fig. 1d** presents the electrostatic potential distribution of the RSC molecule. Notably, the two hydrogen atoms in the phenolic hydroxyl groups are located in the reddest region, corresponding to areas of positive electrostatic potential—indicative of electron-deficient, electrophilic sites capable of chemically adsorbing a anionic iodine species ($I^-/I_3^-/I_5^-$)[30]. Conversely, the two oxygen atoms in the phenolic hydroxyl groups are located in the bluest region, representing areas of negative electrostatic potential—electron-rich, nucleophilic sites that act as electron donors. These features contribute to accelerating the conversion reaction kinetics from polyiodides (I_3^-/I_5^-) to I^- ions[31]. Thus, the phenolic hydroxyl groups in the RSC molecule serve as the functional driving force for both the strong chemical adsorption of polyiodides and their efficient catalytic conversion. **Figs. 1e, S2** respectively present the adsorption and binding energies within iodine species and RSC monomer, while the corresponding adsorption/binding energies are -0.206/-0.206 eV, -1.96/-2.485 eV, -1.047/-1.72 eV, and -2.392/-1.135 eV for I_2, I_5^-, I_3^-, and I^-, suggesting RSC additive holds strong chemisorption capability for polyiodides. To intuitively observe the chemical adsorption effect of RSC on polyiodides, same amount of RSC and ZSO electrolytes are respectively added into the I_3^- solution. Obviously, the color of RSC solution changes from the initial yellow-brown to colorless after standing for 60 min (**Fig. S3**), while the color of ZSO solution does not significantly change.

Additionally, FT-IR spectra are collected for the RSC solution before and after the polyiodide adsorption test. Compared with the pristine RSC solution and RSC powder, a moderate shift in the C-O bond peak is

observed in the RSC solution containing polyiodides (**Fig. S4**). This shift is attributed to the phenolic hydroxyl groups in the RSC molecule, further confirming the presence of chemical interactions between RSC and polyiodides. **Fig. 1f** presents the Gibbs free energy profiles for the stepwise iodine reduction process ($I_2 \rightarrow I_3^- \rightarrow I^-$). Notably, the Gibbs free energy values in both RSC and ZSO electrolytes are negative, indicating that the iodine reduction reactions proceed spontaneously[32]. However, the RSC electrolyte exhibits more negative Gibbs free energy values compared to the ZSO electrolyte, implying that the addition of RSC effectively lowers the reaction energy barrier and accelerates the iodine conversion kinetics[20, 33]. This enhancement is attributed to the strong chemical interactions between the phenolic hydroxyl groups of the RSC molecule and polyiodides. On this basis, as schematically illustrated in **Fig. S5**, the generated I_3^-/I_5^- ions in the RSC electrolyte can be effectively adsorbed, captured, and catalytically converted back into reversible I^- ions during the cycling process. This mechanism disrupts active iodine dissolution, prevents the accumulation of polyiodide concentration gradients at the iodine-loading cathode, and thus suppress the polyiodide shuttle effect in Zn-I_2 batteries. Additionally, due to the strong chemisorption affinity of RSC molecules for iodine species, these conversion reactions are chemically confined to the vicinity of the iodine-loading cathode. This confinement ensures minimal interaction between polyiodides and the zinc anode, thereby reducing zinc corrosion and enhancing the long-term cyclic stability of the Zn-I_2 batteries. In brief, the positive action mechanism of the RSC electrolyte at the iodine-loading cathode can be attributed to the following factors: (1) Strong chemisorption and capture capability for iodine species; (2) effective chemical confinement of iodine conversion reactions to the cathode side; (3) catalytic acceleration of the conversion reaction kinetics from polyiodides (I_3^-/I_5^-) to I^- ions, which collectively suppress active iodine dissolution and inhibit the polyiodide shuttle effect. Building upon the above findings, the chemical interaction mechanism between RSC molecules and polyiodides in the electrolyte can be theoretically inferred as follows: (1) The phenolic hydroxyl groups act as electrophilic sites that chemically capture polyiodides in the electron-deficient region of the RSC molecule; (2) the same groups serve as electron-donating centers in the electron-rich region, catalytically

promoting the conversion from polyiodides (I_3^-/I_5^-) to I- ions; (3) The RSC molecules remain chemically stable and are not consumed during the cycling process.

View Article Online
DOI: 10.1039/D5EE02763B

To verify the practical application of RSC electrolyte, AC@I_2 cathode material is prepared by high-temperature iodine fixation in activated carbon (AC). The similar XRD patterns of AC and AC@I_2 composite suggest the amorphous state of active iodine (**Fig. S6a**)[34], while the thermogravimetric analysis result confirms the iodine loading content in AC@I_2 composite is 49.18 wt.% (**Fig. S6b**). According to the performance comparison of Zn||AC@I_2 batteries in RSC electrolytes with different addition content of RSC, the optimal content is 12 mmol RSC, which well balances the reversible capacity and cyclic stability (**Fig. S7**). **Fig. 2a** contrasts the CV curves of Zn||AC@I_2 batteries in RSC and ZSO electrolytes, where a couple of redox peaks correspond to the reduction ($I_2 \rightarrow I^-$) and oxidation reactions ($I^- \rightarrow I_2$). Notably, Zn||AC@I_2 batteries in RSC electrolyte display narrower redox voltage gap (100 mV *vs*. 190 mV), manifesting faster reaction kinetics[35, 36]. The Tafel slope for the reduction process in different electrolytes are derived from the corresponding LSV curves of Zn||AC@I_2 batteries. As presented in **Fig. 2b**, the calculated Tafel slope of RSC electrolyte (112.44 mV dec^{-1}) is much smaller than that of ZSO electrolyte (180.77 mV dec^{-1}), further confirming that RSC electrolyte can effectively enhance the iodine redox reaction kinetics [23]. Meanwhile, *in-situ* electrochemical impedance spectroscopy (EIS) of Zn||AC@I_2 batteries in RSC and ZSO electrolytes after different cycles are tested (**Figs. 2c, d**). According to the resulting Nyquist plots, the semicircular diameter in middle-high frequency region represents the charge transfer resistances (R_{ct}). The corresponding R_{ct} values of batteries in RSC electrolyte are smaller than that of ZSO electrolyte, and the slopes in the low-frequency region are steeper than that of ZSO electrolyte, indicating that Zn-I_2 batteries in RSC electrolyte hold faster ion transport behavior and faster redox kinetics [37]. Excellent self-discharge resistance capability is one of the key parameters to estimate the sustainable development of Zn||AC@I_2 batteries. As presented in **Fig. S8**, the Coulombic efficiency of AC@I_2 cathode in RSC electrolyte remains 99.0% after two continuous self-discharge cycles, much higher than that in ZSO electrolyte (89.4%), confirming the strengthened anti-self-discharge capability

in RSC electrolyte.

Benefitting from these advantages, both the cyclic stability and rate capability of Zn||AC@I_2 batteries in RSC and ZSO electrolytes are systematically studied. As shown in **Figs. 2e, f**, the cycling behavior of AC@I_2 cathode in RSC and ZSO electrolytes at low temperature and high temperature conditions are also investigated. The reversible capacity of AC@I_2 cathode in RSC electrolyte decreases from 140.2 to 119.9 mA h g^{-1} (-5 ℃), and 175.7 to 145.2 mA h g^{-1} (55 ℃) after 3000 and 1200 cycles at 1 A g^{-1}, respectively, and the corresponding capacity retention rates are as high as 85.5% and 82.6%, indicating RSC electrolyte has good high and low temperature performance. **Figs. 2g, S9** displays the rate capability of Zn||AC@I_2 batteries in RSC electrolyte, and the reversible capacity is 143.9, 137.6, 133.9, 116.7 and 110.6 mA h g^{-1} corresponding to the current density of 0.3, 0.5, 1, 3 and 5 A g^{-1}, which are higher than those of ZSO electrolyte (134.8/130.1/120.3/95.6/84.4 mA h g^{-1}). After reverting to 3, 1, 0.5 and 0.3 A g^{-1}, the capacity can be orderly recovered to 116.4, 133.6, 137.2 and 143.8 mA h g^{-1}, suggesting the superior rate capability in RSC electrolyte. Notably, the reversible capacity of AC@I_2 cathode in RSC electrolyte decreases from 164.4 to 141.1 mA h g^{-1} after 10000 cycles at 1 A g^{-1} at room temperature, corresponding to high-capacity retention ratio of 85.8%. In contrast, the reversible capacity of AC@I_2 cathode in ZSO electrolyte is only 112.1 mA h g^{-1} after 1800 cycles at 1 A g^{-1} (**Fig. 2h**). When the current density rises to 5 A g^{-1}, the discharge capacity of AC@I_2 cathode in RSC electrolyte decreases from 117.9 to 106.2 mA h g^{-1} after 17000 cycles with high-retention ratio of 90.1%, indicating high stability of AC@I_2 cathode in RSC electrolyte at high current density. For the AC@I_2 cathode in ZSO electrolyte, the remained capacity is only 87.8 mA h g^{-1} after 477 cycles at 5 A g^{-1} (**Fig. 2i**). Additionally, the cyclic stability of the AC@I_2 cathode under high iodine loading (3.5 mg cm^{-2}) was evaluated at a current density of 1 A g^{-1} in the RSC electrolyte. As shown in **Fig. S10**, the cathode demonstrates excellent long-term stability, maintaining a high capacity of 134.9 mA h g^{-1} with ahigh capacity retention of 91.5% after 1200 cycles. **Tables S1-S3** comprehensively contrast the cyclic stability and reversible capacity of different iodine-loading cathodes in both coin cells and pouch batteries, while the satisfactory results verify that RSC

electrolyte is conducive to maintain the excellent cycling performances and promote the practical application of Zn||AC@I_2 batteries.

View Article Online
DOI: 10.1039/D5EE02763B

In-situ Raman spectroscopy is adopted to monitor the polyiodide signal intensity of AC@I_2 cathode in RSC and ZSO electrolytes during cycling process. Based on the test results in **Figs. 3a, b, S11**, strong signals of I_3^- and I_5^- species can be respectively detected in AC@I_2 cathode around the positions of 112 and 162 cm^{-1} in ZSO electrolyte[38], which can be attributed to the side reactions between I^- ions and active I_2 component. In sharp contrast, weak polyiodide signal of AC@I_2 cathode is observed in RSC electrolyte at the same position. Meanwhile, trace amounts of polyiodides are obviously observed on the glass fibre separator facing AC@I_2 cathode in ZSO electrolyte (**Fig. S12**), while none in RSC electrolyte, demonstrating the positive role of RSC in suppressing the active iodine dissolution and polyiodide shuttle effect. The iodine intermediates of Zn||AC@I_2 batteries during cycling process are also observed by *in-situ* UV-vis absorption spectra. According to the results in **Figs. 3c-e, S13**, the evident signals of I_3^- species can be detected around the wavelength of 350 nm in ZSO electrolyte[39], and the UV signal of I_3^- species in RSC electrolyte is greatly weakened, suggesting that the introduction of RSC can effectively reduce the generation and concentration of I_3^- species, and thus inhibit the shuttle behavior of polyiodide. H-cell experiments were conducted to further evaluate the ability of RSC to suppress the polyiodide shuttle effect. The left side of H-cell is filled with equal volume of RSC or ZSO electrolytes, and the right side is filled with I_3^- solution, which are physically separated by glass fiber membrane. After standing for 60 min, the color of RSC electrolyte remains almost unchanged (**Fig. 3f**), while obvious color stratification phenomenon occurs in ZSO electrolyte from 15 min to 60 min (**Fig. 3g**), certifying the penetration of I_3^- component into ZSO electrolyte through the glass fibre separator, and the critical role of RSC in capturing polyiodides and inhibiting polyiodide shuttle effect[40].

The molecular orbital analysis of H_2O and RSC molecules are conducted by density functional theory. Generally, the larger energy gap between the lowest unoccupied molecular orbital (LUMO) and the highest occupied molecular orbital (HOMO) represents a more stable electrochemical window. As shown in **Fig. S14a**,

RSC molecule exhibits a smaller energy gap (5.71 eV) than that of H_2O molecule (8.965 eV), implying higher reactivity of RSC molecules[41, 42]. To verify the electrochemical stability of the RSC electrolyte in Zn||AC@I_2 batteries during cycling, both UV-vis absorption spectra and FT-IR spectroscopy were conducted on the RSC electrolyte before and after 50 cycles. As shown in **Fig. S14b**, a distinct absorption peak around 245 nm—attributed to the benzene ring structure in the RSC molecule—remains unchanged after cycling. The near-identical peak positions before and after 50 cycles indicate the inherent electrochemical stability of the benzene ring during the cycling process. Furthermore, the FT-IR spectra in **Fig. S14c** show negligible changes in the characteristic peak of the C-O group, which corresponds to the phenolic hydroxyl groups in the RSC molecule, these results further confirm that the RSC additive retains its chemical integrity and stability throughout the cycling process. The theoretical adsorption energy of RSC molecules on the zinc anode was also calculated. As summarized in **Fig. S15**, the (002) plane of zinc exhibits a stronger adsorption affinity for RSC molecules, with an adsorption energy of -1.901 eV—significantly lower than that of H_2O molecules (-1.615 eV), SO_4^{2-} ions (-1.092 eV), and Zn^{2+} ions (-0.990 eV). This indicates that RSC molecules are preferentially adsorbed on the (002) plane of the zinc anode[7]. Notably, after cycling in the RSC electrolyte, the zinc surface contains a high concentration of carbon and trace amounts of sulfur and iodine, whereas the opposite trend is observed for the ZSO electrolyte (**Figs. S16**). These findings suggest that RSC molecules adsorbed on the zinc surface help suppress the formation of by-products, while those present in the electrolyte contribute to mitigating the polyiodide shuttle effect[43]. Moreover, the solvation environment of Zn^{2+} ions in RSC and ZSO electrolytes was investigated by analyzing the radial distribution functions (RDFs) and coordination number distribution functions (CNDFs) of Zn^{2+} with solvated H_2O molecules and SO_4^{2-} anions through molecular dynamics simulation. As shown in **Figs. 4a, b**, the introduction of the RSC additive significantly reduces the average coordination number of H_2O molecules surrounding Zn^{2+} (from 5.18 to 4.26). This reduction can be attributed to the inherently weak coordination ability of bidentate phenolic hydroxyl groups in RSC, which are capable of forming transient five-membered chelate rings with Zn^{2+} ions,

particularly when partially deprotonated. In parallel, the RSC additive increases the average coordination number of SO_4^{2-} with Zn^{2+} (from 0.82 to 1.62)[44]. Overall, a reduced number of solvated H_2O molecules in the Zn^{2+} solvation structure implies fewer active H_2O molecules are available to corrode the zinc surface during the Zn^{2+} desolvation process. This change in solvation structure helps mitigate by-product and minimizes side reactions on the zinc anode surface.

Fig. S17 and **Table S4** deliver the electrochemical impedance spectra (EIS) of Zn||Zn cells in RSC and ZSO electrolytes at different temperatures (30-55 °C), which can calculate the activation energy (E_a) for the desolvation capability of Zn^{2+} ion. At the same temperature, the R_{ct} of the Zn||Zn cell in RSC electrolyte is lower than that in ZSO electrolyte. The corresponding E_a values are calculated based on the Arrhenius equation. The E_a value of Zn anode in RSC electrolyte (40.74 kJ mol^{-1}) is lower than that in ZSO electrolyte (45.35 kJ mol^{-1}, **Fig. 4c**)[45], implying that RSC electrolyte reduces the energy barrier of Zn^{2+} desolvation process and accelerates the Zn^{2+} desolvation kinetics. Furthermore, **Fig. S18** presents the Gibbs free energy profiles of the stepwise desolvation of $Zn(H_2O)_xSO_4$ in both RSC and ZSO electrolytes, highlighting the differences in Zn^{2+} desolvation behavior. Upon the introduction of the RSC additive, the initial solvation configuration of Zn^{2+} ion transforms from $Zn(H_2O)_5SO_4$ to $Zn(H_2O)_3SO_4$. This shift results in fewer desolvation steps and lower Gibbs free energy barriers, demonstrating the enhanced capability of RSC to facilitate the removal of coordinated H_2O molecules from the Zn^{2+} solvation shell[46]. **Fig. 4d** compares the corrosion resistance of zinc metal in RSC and ZSO electrolytes by Tafel curves, and the corrosion current density decreases from 1.748 mA cm^{-2} to 0.441 mA cm^{-2} with the introduction of RSC additive, suggesting the inhibited corrosion processes and the enhanced stability of zinc metal in RSC electrolyte[47]. Zn||Ti cells are assembled to evaluate the inhibition of hydrogen evolution reaction by the corresponding LSV curves. As depicted in **Fig. 4e**, the hydrogen evolution potential in the RSC electrolyte (-0.13 V) is lower than that in the ZSO electrolyte (-0.10 V), indicating that the hydrogen evolution reaction is more difficult to initiate in the RSC electrolyte. To further validate this conclusion, three-electrode LSV measurements were conducted using

Zn||Ti cells in three different electrolytes: RSC-containing K_2SO_4 electrolyte, ZSO, and RSC electrolyte. As summarized in **Figs. S19**, the RSC-containing electrolytes consistently exhibit lower hydrogen evolution potentials, regardless of the presence of Zn^{2+} ions. These results clearly demonstrate that the introduction of RSC additive effectively suppresses the hydrogen evolution reaction[47]. The contact angle of ZSO electrolyte on Zn anode is 95°, showing poor wettability. In contrast, the contact angle of RSC electrolyte on Zn anode is reduced to 63°, indicating that the wettability is significantly improved (**Fig. S20**)[42]. Chronoamperometry (CA) curves of Zn||Zn cells in RSC and ZSO electrolytes are implemented to study the reaction kinetic behavior. As displayed in **Fig. S21**, the current density of Zn anode in RSC is higher than that in ZSO electrolyte, indicating that the Zn^{2+} ions are dispersed more quickly on Zn anode in RSC electrolyte, which is beneficial to the uniform zinc deposition behavior[48, 49].

As shown in **Figs. S22, S23**, the Zn||Zn cells in RSC electrolyte achieve stable cycling behavior for 520 h under the condition of 0.1 mA cm^{-2} and 0.1 mA h cm^{-2}, as well as 350 h under the condition of 3 mA cm^{-2} and 1 mA h cm^{-2} without short circuit phenomenon. In contrast, the corresponding voltage polarization hysteresis curves in ZSO electrolyte present obvious abnormal fluctuation only after 60 h at the condition of 0.1 mA cm^{-2} and 0.1 mA h cm^{-2}, elucidating the positive role of RSC additive in stabilizing the interface reaction of zinc metal[50]. The assembled Zn||Cu cells in the RSC electrolyte exhibit stable zinc deposition behavior and a high average Coulombic efficiency of 99.23% over 350 cycles under a current density of 2 mA cm^{-2} and an areal capacity of 1 mA h cm^{-2}, demonstrating highly reversible Zn plating/stripping behavior (**Fig. S24**)[31]. The formation of by-product ($Zn_4SO_4(OH)_6{\cdot}5H_2O$) is one of the key factors affecting the long-term stability. The zinc surface after 20 cycles is detected by atomic force microscopy (AFM), XRD and SEM techniques. Notably, larger surface topographical variations appear in ZSO electrolyte, while relatively smooth surface in RSC electrolyte (**Figs. 4f, g**). XRD patterns further manifest the formation of by-products on Zn foil in ZSO electrolyte, while negligible by-products on Zn foil in RSC electrolyte (**Fig. S25**)[51]. After several days immersion test in different electrolyte environments (RSC/ZSO/RSC+I_3^-/ZSO+I_3^-), the zinc

surface in RSC-containing electrolyte remains smooth and non-corrosive morphology, while flake-like by-products and serious corrosion phenomena appear in ZSO-containing electrolyte (**Figs. 4h, i, S26**), demonstrating the protective effect of RSC additive on Zn anode.

To evaluate the practical application of RSC additive[52], Zn||AC@I_2 pouch batteries are assembled (**Fig. S27**), and the size of each pouch battery is 5 cm × 5 cm. **Fig. S28** tests the cycling performance of pouch battery in RSC electrolyte with high iodine loading of 10.8 mg cm^{-2}. The reversible capacity of AC@I_2 cathode decreases from 178.0 to 169.8 mA h g^{-1} after 350 cycles at 0.5 A g^{-1}, corresponding to the high-capacity retention ratio of 95.4%. As presented in **Fig. S29**, the corresponding pouch battery assembled with a 100 μm Zn foil anode and a high-iodine loading cathode of 26.8 mg cm^{-2}, exhibits a stable areal capacity of 4.06 mA h cm^{-2} with negligible capacity decay over 60 cycles at 0.5 A g^{-1}, further demonstrating the practical potential of the RSC additive. To comprehensively assess the advantages of the RSC electrolyte under extremely low negative/ positive (N/P) ratio conditions, thin Zn foil anode (20 μm), high-iodine loading cathodes of 12.7 and 22.8 mg cm^{-2} were utilized to assemble the Zn||AC@I_2 pouch batteries. As a result, the assembled pouch battery with iodine loading cathode of 12.7 mg cm^{-2} (N/P=4.4) delivers high-capacity retention rate of 97.9% at 0.5 A g^{-1}, corresponding to the discharge capacity decrease from 169.4 to 165.8 mA h g^{-1} after 200 cycles (**Figs. 5a, b**). Meanwhile, the assembled pouch battery with iodine loading cathode of 22.8 mg cm^{-2} (N/P=2.5) holds stable areal capacity of 3.53 mA h cm^{-2} after 200 cycles at 0.5 A g^{-1} (**Figs. 5c, d**). As delivered in **Figs. 5e, S30**, the pouch battery assembled with thick Zn foil anode (100 μm) and high-iodine loading cathode of 14.1 mg cm^{-2}, displays high reversible capacity of 180.8, 169.7, 167.8, 155.1, 128.5 and 90.0 mA h g^{-1} at 0.3, 0.4, 0.5, 1.0, 2.0 and 3.0 A g^{-1}, respectively. These results indicate the introduction of RSC additive can effectively alleviate the poor cyclic stability and short lifespan of Zn||AC@I_2 batteries. To further assess the practicality and safety of RSC electrolyte, three Zn||AC@I_2 pouch batteries are connected in series, which can yield stable working voltage of 3.57 V (**Fig. 5f**) and light up an LED panel with characters of "HNU" (**Fig. 5g**). When the pouch batteries are bent at 90°, 180°, punctured and even cut, there is no significant change in

the battery voltage (**Fig. S31**). The Zn||AC@I_2 pouch batteries can also maintain the normal operation of LED panel without emitting smoke or flame even at piercing (**Fig. 5h**) and cutting (**Fig. 5i**) states[53], demonstrating the significant safety advantages of Zn||AC@I_2 batteries in RSC electrolyte.

3. Conclusion

In summary, this study demonstrates the effectiveness of RSC as an electrolyte additive in enhancing the cycling stability of Zn-I_2 batteries. The strong chemical interaction within RSC and iodine species effectively accelerates the iodine conversion reaction kinetics, inhibits the formation and shuttle of polyiodides on iodine loading cathode, and mitigate parasitic side reactions on zinc anode. As a result, Zn||Zn cells in RSC electrolyte deliver remarkable zinc plating/stripping behavior, and Zn||AC@I_2 batteries in RSC electrolyte exhibit durable cycling stability for 17000 cycles at 5 A g^{-1} with high-capacity retention rate of 90.1%. The assembled pouch batteries also achieve excellent electrochemical performance even under high iodine loading conditions, demonstrating the viability of RSC additive as cost-effective solution for active iodine dissolution and polyiodide shuttle effect. This work not only offers an efficient approach to improve the performance of Zn-I_2 batteries, but also provides deep insight for the electrolyte design to accelerate the commercialization of aqueous zinc batteries.

Author Contributions

Zhixiang Chen: Conceptualization, Data curation, Methodology, Investigation, Writing-original draft; **Xinlei Gao**: Conceptualization, Methodology, Formal analysis, Validation; **Lutong Shan**: Software, Validation, Visualization; **Qingjin Fu**: Formal analysis, Visualization; **Zhenyue Xing**: Resources, Funding acquisition; **Peng Rao**: Data curation, Funding acquisition; **Zhenye Kang**: Methodology, Funding acquisition; **Xiaodong Shi**: Conceptualization, Methodology, Funding acquisition, Writing-review & editing, Supervision; **Wei Zhang**: Data curation, Formal analysis, Writing-original draft, Supervision; **Xinlong Tian**: Resources, Funding acquisition, Writing-review & editing, Supervision, Project administration.

Conflict of Interest

The authors declare no competing interests.

Acknowledgments

The authors thank the National Natural Science Foundation of China (52404316, 52461040, and 52274297), Collaborative Innovation Center of Marine Science and Technology of Hainan University (XTCX2022HYC14), and Start-up Research Foundation of Hainan University (XJ2400012968, KYQD(ZR)-23069, 23169, and 21124). Additionally, the authors acknowledge the support for comprehensive characterizations by Pico Election Microscopy Center of Hainan University.

Supporting Information

Supporting Information is available from the authors.

References

(1) Zhang, L.; Ding, H.; Gao, H.; Gong, J.; Guo, H.; Zhang, S.; Yu, Y.; He, G.; Deng, T.; Parkin, I. P.; et al. An integrated design for high-energy, durable zinc-iodine batteries with ultra-high recycling efficiency. *Energy Environ. Sci.* **2025**, *18* (5), 2462-2473.

(2) Yan, W.; Liu, Y.; Qiu, J.; Tan, F.; Liang, J.; Cai, X.; Dai, C.; Zhao, J.; Lin, Z. A tripartite synergistic optimization strategy for zinc-iodine batteries. *Nat. Commun.* **2024**, *15* (1), 9702.

(3) Chen, H.; Li, X.; Fang, K.; Wang, H.; Ning, J.; Hu, Y. Aqueous zinc-iodine batteries: from electrochemistry to energy storage mechanism. *Adv. Energy Mater.* **2023**, *13* (41), 2302187.

(4) Cao, S.; Zhang, A.; Fang, H.; Feng, B.; Liu, Y.; Yi, P.; He, S.; Ren, Z.; Ma, L.; Lu, W.; et al. Skin-like quasi-solid-state electrolytes for spontaneous zinc-ion dehydration toward ultra-stable zinc-iodine batteries. *Energy Environ. Sci.* **2025**, *18 (7)*, 3395-3406.

(5) Gupta, D.; Liu, S.; Zhang, R.; Guo, Z. Future Long Cycling Life Cathodes for Aqueous zinc-ion batteries in grid-Scale energy storage. *Adv. Energy Mater.* **2025**, *15*, 2500171.

(6) Chen, Q.; Hao, J.; Zhu, Y.; Zhang, S. J.; Zuo, P.; Zhao, X.; Jaroniec, M.; Qiao, S. Z. Anti-swelling microporous membrane for high-capacity and long-life Zn−I_2 batteries. *Angew. Chem. Int. Ed.* **2025**, *64* (1), e202413703.

(7) Chen, J.; Ou, G.; Liu, P.; Fan, W.; Li, B.; Hu, Z.; Wen, Z.; Zhang, Y.; Tang, Y.; Liu, X.; et al. Pyrrolic-nitrogen chemistry in 1-(2-hydroxyethyl)imidazole electrolyte additives toward a 50,000-cycle-Life aqueous zinc-iodine battery. *Angew. Chem. Int. Edit.* **2025**, *64* (2), e202414166.

(8) Liu, Y.; Zhang, L.; Liu, L.; Ma, Q.; Wang, R.; Xiong, P.; Li, H.; Zhang, S.; Hao, J.; Zhang, C. All-climate energy-dense cascade aqueous Zn-I_2 batteries enabled by a polycationic hydrogel electrolyte. *Adv. Mater.* **2025**, 2415979. DOI: https://doi.org/10.1002/adma.202415979

(9) Chen, Z.; Wang, F.; Ma, R.; Jiao, W.; Li, D.; Du, A.; Yan, Z.; Yin, T.; Yin, X.; Li, Q.; et al. Molecular

catalysis enables fast polyiodide conversion for exceptionally long-life zinc-iodine batteries. *ACS Energy Lett.* **2024**, *9* (6), 2858-2866.

View Article Online
DOI: 10.1039/D5EE02763B

(10) Liu, T.; Lei, C.; Yang, W.; Wang, H.; Ma, W.; Li, J.; Liang, X. Solvent chemistry manipulated iodine redox thermodynamics for durable iodine batteries. *Angew. Chem. Int. Edit.* **2025**, *64*, e202422163.

(11) Li, F.; Zhou, C.; Zhang, J.; Gao, Y.; Nan, Q.; Luo, J.; Xu, Z.; Zhao, Z.; Rao, P.; Li, J.; et al. Mullite mineral-derived robust solid electrolyte enables polyiodide shuttle-free zinc-iodine batteries. *Adv. Mater.* **2024**, *36* (38), 2408213.

(12) Wang, K.; Li, H.; Xu, Z.; Liu, Y.; Ge, M.; Wang, H.; Zhang, H.; Lu, Y.; Liu, J.; Zhang, Y.; et al. An iodine-chemisorption binder for high-loading and shuttle-free Zn-iodine batteries. *Adv. Energy Mater.* **2024**, *14* (17), 2304110.

(13) Dong, C.; Yu, Y.; Ma, C.; Zhou, C.; Wang, J.; Gu, J.; Ji, J.; Yang, S.; Liu, Z.; Xu, X.; et al. Tailoring zinc diatomic bidirectional catalysts achieving orbital coupling-hybridization for ultralong-cycling zinc-iodine batteries. *Energy Environ. Sci.* **2025**, *18*, 3014-3025.

(14) Yang, J.; Zhao, R.; Wang, Y.; Hu, Z.; Wang, Y.; Zhang, A.; Wu, C.; Bai, Y. Insights on artificial interphases of Zn and electrolyte: protection mechanisms, constructing techniques, applicability, and prospective. *Adv. Funct. Mater.* **2023**, *33* (14), 2213510.

(15) Tan, L.; Wei, J.; Xue, L.; Luo, D.; Chen, G.; Chu, Y.; Wang, J.; Zong, K.; Song, X.; Yang, L.; et al. Regulating the electron structure of covalent organic frameworks to enable excellent cycle life and high rate toward advanced Zn-I_2 batteries. *Adv. Funct. Mater.* **2025**, *35*, 2416931.

(16) Yang, J.; Zhao, R.; Hu, Z.; Wang, Y.; Zhang, K.; Wang, Y.; Han, X.; Zhang, A.; Wu, C.; Bai, Y. Blocking the passivation reaction via localized acidification and cation selective interface towards highly stable zinc anode. *Energy Storage Mater.* **2024**, *70*, 103449.

(17) Zhang, H.; Gan, X.; Gao, Y.; Wu, H.; Song, Z.; Zhou, J. Carboxylic acid-functionalized cellulose hydrogel electrolyte for dual-interface stabilization in aqueous zinc-organic batteries. *Adv. Mater.* **2025**, *37* (1), 2411997.

(18) Chen, G.; Kang, Y.; Yang, H.; Zhang, M.; Yang, J.; Lv, Z.; Wu, Q.; Lin, P.; Yang, Y.; Zhao, J. Toward forty thousand-cycle aqueous zinc-iodine battery: simultaneously inhibiting polyiodides shuttle and stabilizing zinc anode through a suspension electrolyte. *Adv. Funct. Mater.* **2023**, *33* (28), 2300656.

(19) Gao, Y.; Liu, Y.; Guo, X.; Zhang, J.; Zhou, C.; Li, F.; Xu, Z.; Zhao, Z.; Xing, Z.; Rao, P.; et al. Trimetallic atom-doped functional carbon catalyst enables fast redox kinetics and durable cyclic stability of zinc-iodine batteries. *Adv. Funct. Mater.* **2025**, *35*, 2421714.

(20) Zhao, Y.; Wang, Y.; Xue, W.; Cheng, R.; Zheng, X.; Zhu, G.; Hu, D.; Huang, H.; Hu, C.; Liu, D.

Unveiling the role of cationic pyridine sites in covalent triazine framework for boosting zinc-iodine batteries performance. *Adv. Mater.* **2024**, *36* (31), 2403097.

View Article Online
DOI: 10.1039/D5EE02763B

(21) Liu, M.; Chen, Q.; Cao, X.; Tan, D.; Ma, J.; Zhang, J. Physicochemical confinement effect enables high-performing zinc-iodine batteries. *J. Am. Chem. Soc.* **2022**, *144* (47), 21683-21691.

(22) Qu, W.; Yuan, Y.; Wen, C.; Zhu, J.; Liang, X.; Chen, S.; Li, Z.; Cao, G.; Zhang, M. Ultra-long life and high rate performance zinc-iodine batteries simultaneously enabled by a low-spin electrode. *Energy Storage Mater.* **2025**, *75*, 103993.

(23) He, J.; Mu, Y.; Wu, B.; Wu, F.; Liao, R.; Li, H.; Zhao, T.; Zeng, L. Synergistic effects of lewis acid-base and coulombic interactions for high-performance Zn-I_2 batteries. *Energy Environ. Sci.* **2024**, *17* (1), 323-331.

(24) Yang, P.; Zhang, K.; Liu, S.; Zhuang, W.; Shao, Z.; Zhu, K.; Lin, L.; Guo, G.; Wang, W.; Zhang, Q.; et al. Ionic selective separator design enables long-life zinc-iodine batteries via synergistic anode stabilization and polyiodide shuttle suppression. *Adv. Funct. Mater.* **2024**, *34* (52), 2410712.

(25) Liao, X.; Zhu, Z.; Liao, Y.; Fu, K.; Duan, Y.; Lv, L.; Wu, L.; Wang, W.; He, X.; Yang, K.; et al. Cation adsorption engineering enables dual stabilizations for fast-charging Zn-I_2 batteries. *Adv. Energy Mater.* **2024**, *14* (47), 2402306.

(26) Fu, Q.; Zhang, W.; Liu, X.; Liu, Y.; Lei, Z.; Zhang, M.; Qu, H.; Xiao, X.; Zhong, X.; Liu, Z.; et al. Dynamic imine chemistry enables paintable biogel electrolytes to shield on-body zinc-ion batteries from interfacial interference. *J. Am. Chem. Soc.* **2024**, *146* (50), 34950-34961.

(27) Yang, H.; Qiao, Y.; Chang, Z.; Deng, H.; Zhu, X.; Zhu, R.; Xiong, Z.; He, P.; Zhou, H. Reducing water activity by zeolite molecular sieve membrane for long-life rechargeable zinc battery. *Adv. Mater.* **2021**, *33* (38), 2102415.

(28) Yang, C.; Woottapanit, P.; Geng, S.; Chanajaree, R.; Lolupiman, K.; Limphirat, W.; Zhang, X.; Qin, J. Biomimetic inorganic-organic protective layer for highly stable and reversible Zn anodes. *ACS Energy Lett.* **2025**, *10* (1), 337-344.

(29) He, H.; Qin, H.; Wu, J.; Chen, X.; Huang, R.; Shen, F.; Wu, Z.; Chen, G.; Yin, S.; Liu, J. Engineering interfacial layers to enable Zn metal anodes for aqueous zinc-ion batteries. *Energy Storage Mater.* **2021**, *43*, 317-336.

(30) Chen, Z.; Zhang, J.; Zhou, C.; Guo, S.; Wu, D.; Zhao, Z.; Wang, Z.; Li, J.; Xing, Z.; Rao, P.; et al. Sulfonated lignin binder blocks active iodine dissolution and polyiodide shuttle toward durable zinc-iodine batteries. *Adv. Energy Mater.* **2025**, *15* (8), 2404814.

(31) Zhang, L.; Huang, J.; Guo, H.; Ge, L.; Tian, Z.; Zhang, M.; Wang, J.; He, G.; Liu, T.; Hofkens, J.; et al. Tuning ion transport at the anode-electrolyte interface via a sulfonate-rich ion-exchange layer for durable zinc-

iodine batteries. *Adv. Energy Mater.* **2023**, *13* (13), 2203790.

(32) Hu, T.; Zhao, Y.; Yang, Y.; Lv, H.; Zhong, R.; Ding, F.; Mo, F.; Hu, H.; Zhi, C.; Liang, G. Development of inverse-opal-structured charge-deficient Co_9S_8@nitrogen-doped-carbon to catalytically enable high energy and high power for the two-electron transfer I^+/I^- electrode. *Adv. Mater.* **2024**, *36* (18), 2312246.

(33) Yang, F.; Long, J.; Yuwono, J. A.; Fei, H.; Fan, Y.; Li, P.; Zou, J.; Hao, J.; Liu, S.; Liang, G.; et al. Single atom catalysts for triiodide adsorption and fast conversion to boost the performance of aqueous zinc-iodine batteries. *Energy Environ. Sci.* **2023**, *16* (10), 4630-4640.

(34) Sun, H.; Li, M.; Zhu, J.; Ni, J.; Li, L. Capitalizing on the iodometric reaction for energetic aqueous energy storage. *ACS Nano* **2024**, *18* (32), 21472-21479.

(35) Zhang, S. J.; Hao, J.; Wu, H.; Chen, Q.; Ye, C.; Qiao, S .Z. Protein interfacial gelation toward shuttle-free and dendrite-free Zn-iodine batteries. *Adv. Mater.* **2024**, *36* (35), 2404011.

(36) Liang, G.; Liang, B.; Chen, A.; Zhu, J.; Li, Q.; Huang, Z.; Li, X.; Wang, Y.; Wang, X.; Xiong, B.; et al. Development of rechargeable high-energy hybrid zinc-iodine aqueous batteries exploiting reversible chlorine-based redox reaction. *Nat. Commun.* **2023**, *14* (1), 1856.

(37) Nason, C. A. F.; Vijaya Kumar Saroja, A. P.; Lu, Y.; Wei, R.; Han, Y.; Xu, Y. Layered potassium titanium niobate/reduced graphene oxide nanocomposite as a potassium-ion battery anode. *Nano-Micro Lett.* **2024**, *16* (1), 1.

(38) Li, B.; Nie, Z.; Vijayakumar, M.; Li, G.; Liu, J.; Sprenkle, V.; Wang, W. Ambipolar zinc-polyiodide electrolyte for a high-energy density aqueous redox flow battery. *Nat. Commun.* **2015**, *6* (1), 6303.

(39) Li, D.; Zhu, Y. J.; Cheng, L.; Xie, S.; Yu, H. P.; Zhang, W.; Xu, Z.; Ma, M. G.; Li, H. A MXene modulator enabled high-loading iodine composite cathode for stable and high-energy-density Zn-I_2 battery. *Adv. Energy Mater.* **2024**, *n/a* (n/a), 2404426. DOI: https://doi.org/10.1002/aenm.202404426

(40) Xu, Y.; Zhang, M.; Tang, R.; Li, S.; Sun, C.; Lv, Z.; Yang, W.; Wen, Z.; Li, C. C.; Li, X.; et al. A plant root cell-inspired interphase layer for practical aqueous zinc-iodine batteries with super-high areal capacity and long lifespan. *Energy Environ. Sci.* **2024**, *17* (18), 6656-6665.

(41) Fu, H.; Huang, S.; Wang, T.; Lu, J.; Xiong, P.; Yao, K.; Byun, J. S.; Li, W.; Kim, Y.; Park, H. S. Synergistic cationic shielding and anionic chemistry of potassium hydrogen phthalate for ultrastable Zn-I_2 full batteries. *Adv. Mater.* **2025**, *37* (3), 2411686.

(42) Chen, Z.; Jiang, R.; Chen, Y.; Zhu, H.; Tang, X.; Huang, X.; Xie, Y.; Li, J.; Zhang, C.; Chen, L.; et al. Zincophilic group-rich aminoglycosides for ultra-long life and high-rate zinc batteries. *Energy Storage Mater.* **2025**, *74*, 103913.

(43) Zhang, L.; Luo, K.; Gong, J.; Zhou, Y.; Guo, H.; Yu, Y.; He, G.; Gohy, J. F.; Parkin, I. P.; Hofkens, J.;

et al. Unlocking durable and sustainable zinc-iodine batteries via molecularly engineered polyiodide reservoirs. *Angew. Chem. Int. Ed.* **2025**, *n/a (n/a)*, e202506822. DOI: https://doi.org/10.1002/anie.202506822

(44) Liu, Q.; Liu, X.; Liu, Y.; Huang, M.; Wang, W.; Cheng, Y.; Zhang, H.; Xu, L. Atomic-level customization of zinc crystallization kinetics at the interface for high-utilization Zn anodes. *ACS Nano* **2024**, *18* (6), 4932-4943.

(45) Zhao, X.; Fu, J.; Chen, M.; Wang, Y.; Huang, C.; Qian, K.; Feng, G.; Li, B.; Zhou, D.; Kang, F. A self-phase separated electrolyte toward durable and rollover-stable zinc metal batteries. *J. Am. Chem. Soc.* **2025**, *147* (3), 2714-2725.

(46) Wu, A.; Zhang, S.; Li, Q.; Xue, W.; Li, C.; Xi, B.; Mao, W.; Bao, K.; Xiong, S. Multifunctional crown ether additive regulates desolvation process to achieve highly reversible zinc-metal batteries. *Adv. Energy Mater.* **2025**, 15, 2404450.

(47) Wang, Y.; Zhao, R.; Liu, M.; Yang, J.; Zhang, A.; Yue, J.; Wu, C.; Bai, Y. Suppressed water reactivity by zincophilic-hydrophobic electrolyte additive for superior aqueous Zn metal batteries. *Adv. Energy Mater.* **2023**, *13* (43), 2302707.

(48) Zeng, Y.; Zhang, X.; Qin, R.; Liu, X.; Fang, P.; Zheng, D.; Tong, Y.; Lu, X. Dendrite-free zinc deposition induced by multifunctional CNT frameworks for stable flexible Zn-ion batteries. *Adv. Mater.* **2019**, *31* (36), 1903675.

(49) Chen, J.; Liu, N.; Zhao, S.; Dong, W.; Lv, Z.; Wan, D.; Bi, H.; Huang, F. Zincophilic tellurium interface layer enables fast kinetics for ultralow overpotential and highly reversible zinc anode. *Adv. Funct. Mater.* **2025**, *35* (3), 2413495.

(50) Chen, R.; Zhang, W.; Guan, C.; Zhou, Y.; Gilmore, I.; Tang, H.; Zhang, Z.; Dong, H.; Dai, Y.; Du, Z.; et al. Rational design of an in-situ polymer-inorganic hybrid solid electrolyte interphase for realising stable Zn metal anode under harsh conditions. *Angew. Chem. Int. Ed.* **2024**, *63*, e202401987.

(51) Wang, F.; Liang, W.; Liu, X.; Yin, T.; Chen, Z.; Yan, Z.; Li, F.; Liu, W.; Lu, J.; Yang, C.; et al. A bifunctional electrolyte additive features preferential coordination with iodine toward ultralong-life zinc-iodine batteries. *Adv. Energy Mater.* **2024**, *14* (21), 2400110.

(52) Zong, Y.; Chen, H.; Wang, J.; Wu, M.; Chen, Y.; Wang, L.; Huang, X.; He, H.; Ning, X.; Bai, Z.; Wen, W.; Zhu, D.; Ren, X.; Wang, N.; Dou, S., Cation defect-engineered boost fast kinetics of two-dimensional topological Bi_2Se_3 cathode for high-performance aqueous Zn-ion batteries. *Adv. Mater.* **2023**, *35* (51), 2306269.

(53) Bu, J.; Liu, P.; Ou, G.; Ye, M.; Wen, Z.; Zhang, Y.; Tang, Y.; Liu, X.; Li, C. C., Interfacial adsorption layers based on amino acid analogues to enable dual stabilization toward long-life aqueous zinc iodine

batteries. *Adv. Mater.* **2025**, *37* (19), 2420221.

View Article Online
DOI: 10.1039/D5EE02763B

Figures and captions

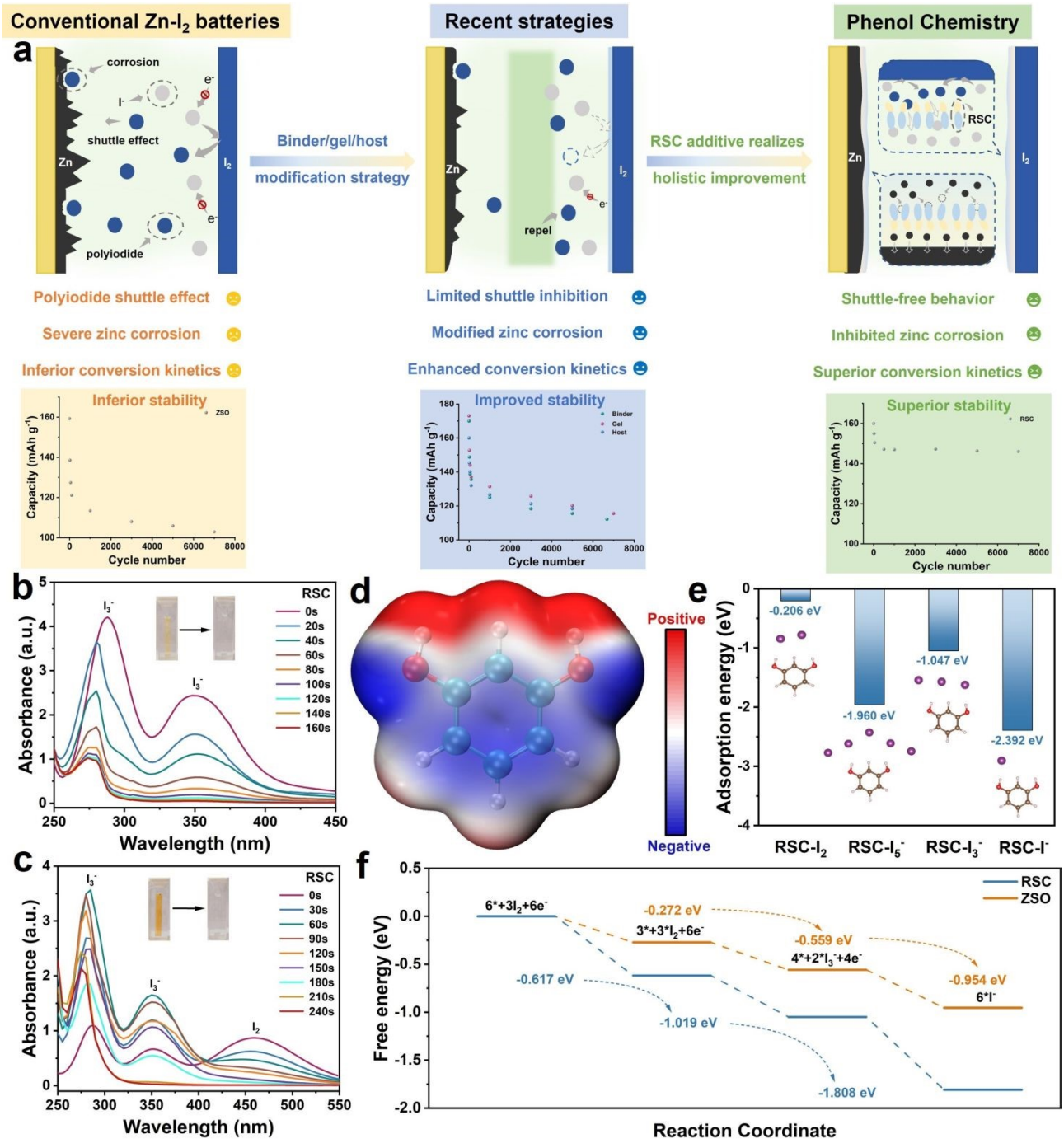

Figure 1 (a) Schematic comparison of action mechanism of RSC additive on the Zn-I_2 batteries; UV-vis absorption spectra of RSC-containing solution (b) during I_3^- adsorption process and (c) during I_2 adsorption process; (d) Electrostatic potential distribution of RSC molecule; (e) The calculated adsorption energy and the corresponding adsorption models of I_2, I_5^-, I_3^- and I^- species on the monomer structure of RSC molecule; (f)

Gibbs free energy values for the consecutive iodine reduction reaction driven by different electrolytes.

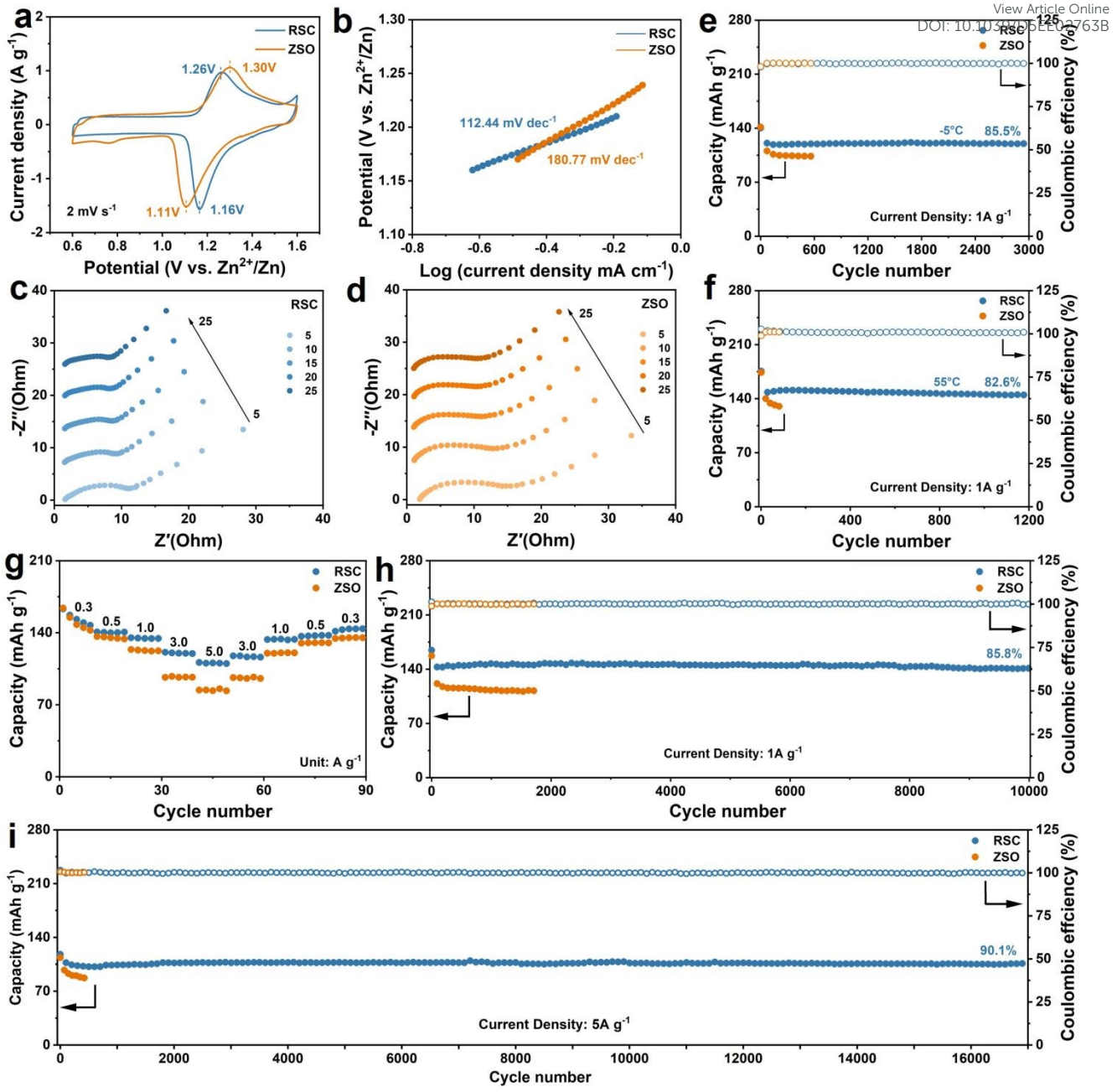

Figure 2 (a) Normalized CV curves of Zn||AC@I_2 batteries at 2 mV s^{-1} in different electrolytes; (b) Tafel plots of Zn||AC@I_2 batteries in different electrolytes corresponding to the polarization curves; *In-situ* electrochemical impedance spectroscopy of Zn||AC@I_2 batteries in (c) RSC and (d) ZSO electrolytes after different cycles; Cyclic performances of Zn||AC@I_2 batteries at 1 A g^{-1} (e) at low temperature of -5 ℃ and (f) at high temperature of 55 ℃ in different electrolytes; (g) Rate performances of Zn||AC@I_2 batteries in different electrolytes at the current densities of 0.3, 0.5, 1, 3 and 5 A g^{-1}; Long-term cyclic stability of Zn||AC@I_2

batteries in different electrolytes at high current densities of (h) 1 A g^{-1} and (i) 5 A g^{-1}.

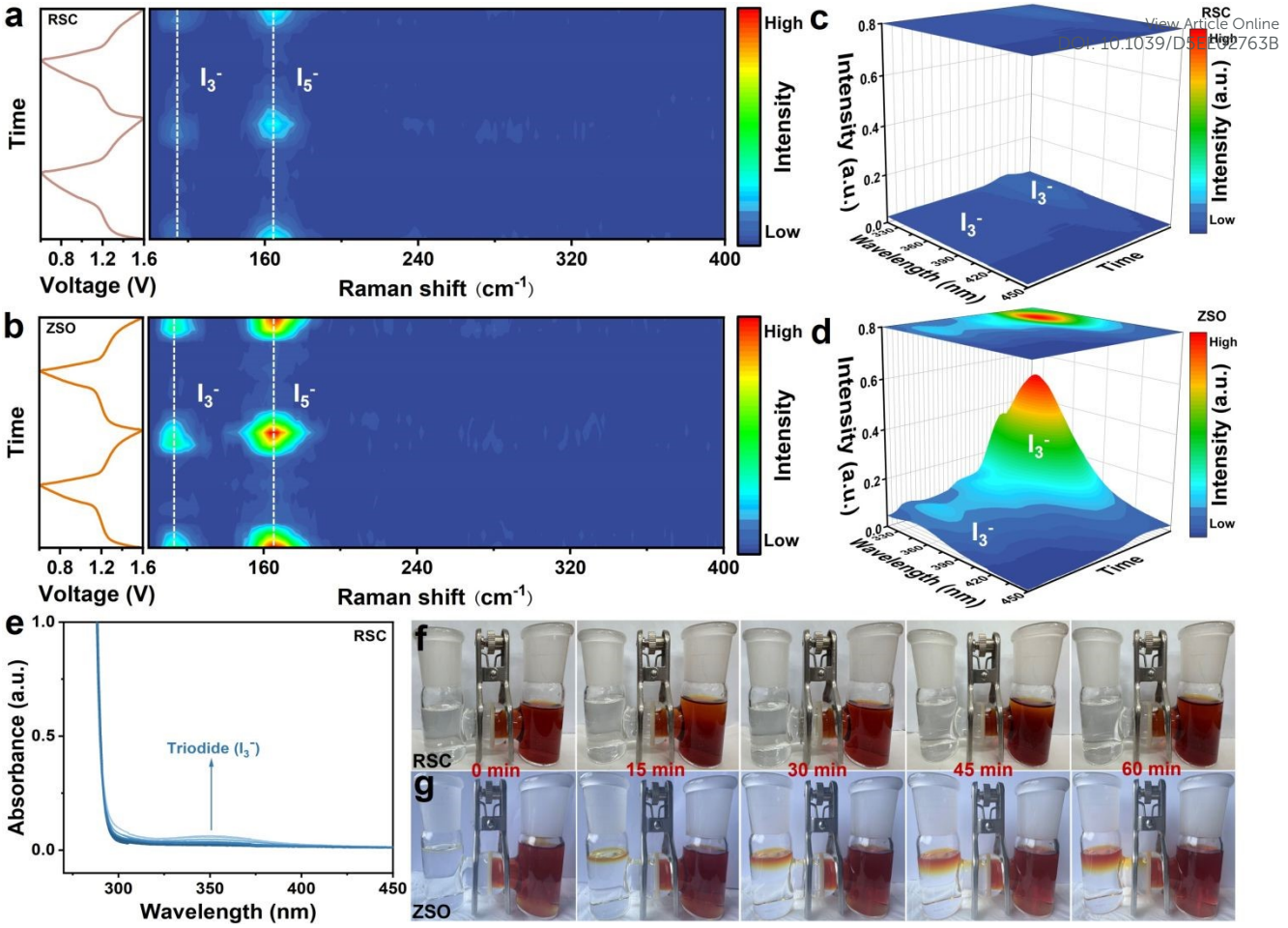

Figure 3 *In-situ* Raman spectra of Zn||AC@I_2 batteries during cycling process in (a) RSC and (b) ZSO electrolytes; *In-situ* UV-vis absorption spectra of Zn||AC@I_2 batteries during cycling process in (c) RSC and (d) ZSO electrolytes; (e) The corresponding UV-vis absorbance intensity of Zn||AC@I_2 batteries during cycling process in RSC electrolyte; Penetration tests of I_3^- solution through the glass fibre separator to (f) RSC and (g) ZSO electrolytes.

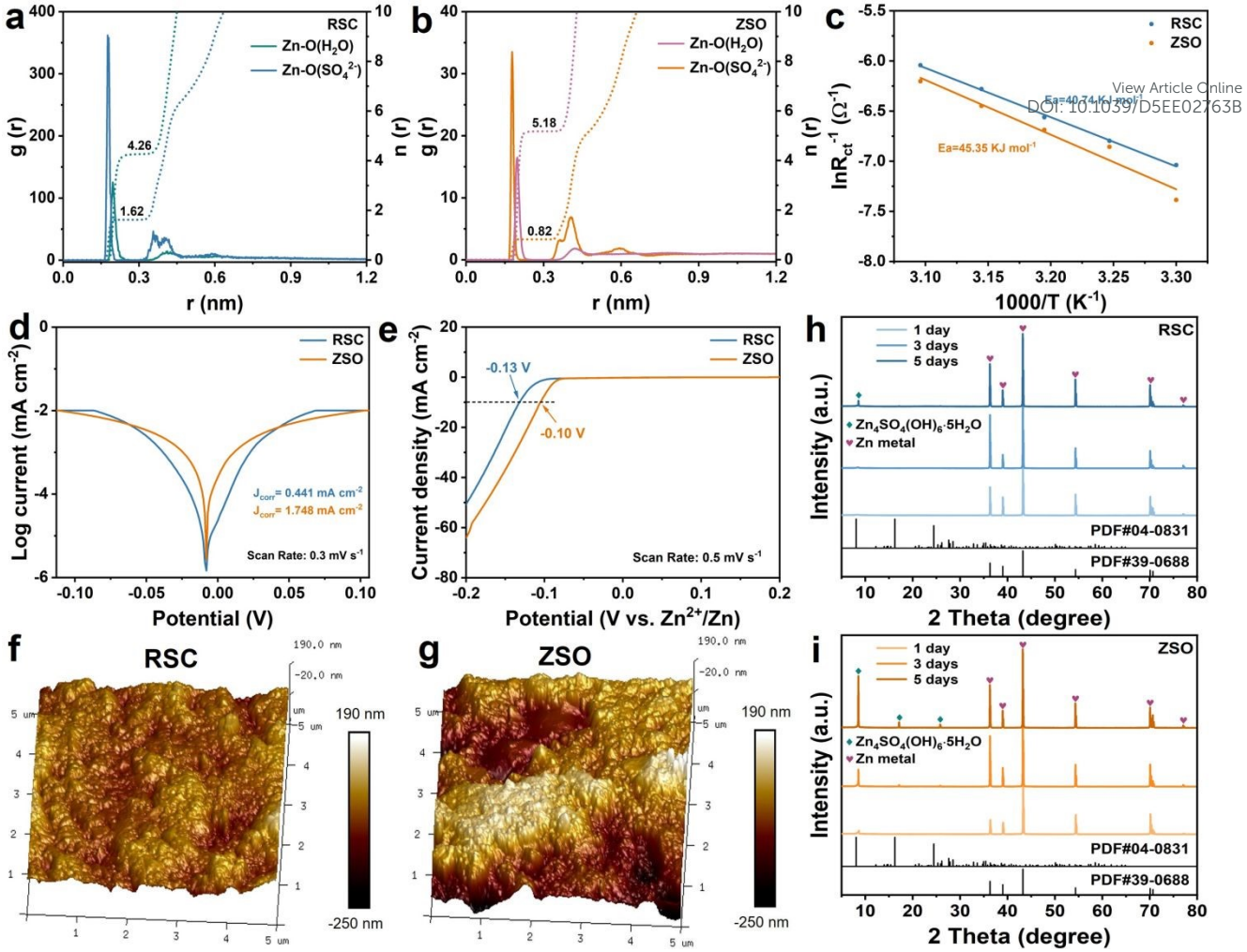

Figure 4 Radial distribution functions (RDFs) and coordination number distribution functions (CNDFs) of (a) RSC and (b) ZSO electrolytes; (c) The calculated activation energy barriers of Zn||Zn cells in RSC and ZSO electrolytes; (d) Tafel curves of Zn||Zn cells in RSC and ZSO electrolytes; (e) Linear sweep voltammetry (LSV) curves of Zn||Ti cells in RSC and ZSO electrolytes; Atomic force microscope (AFM) images of the post-cycling Zn anodes in (f) RSC and (g) ZSO electrolytes; XRD patterns of Zn metal immersed in (h) RSC and (i) ZSO electrolytes for 5 days.

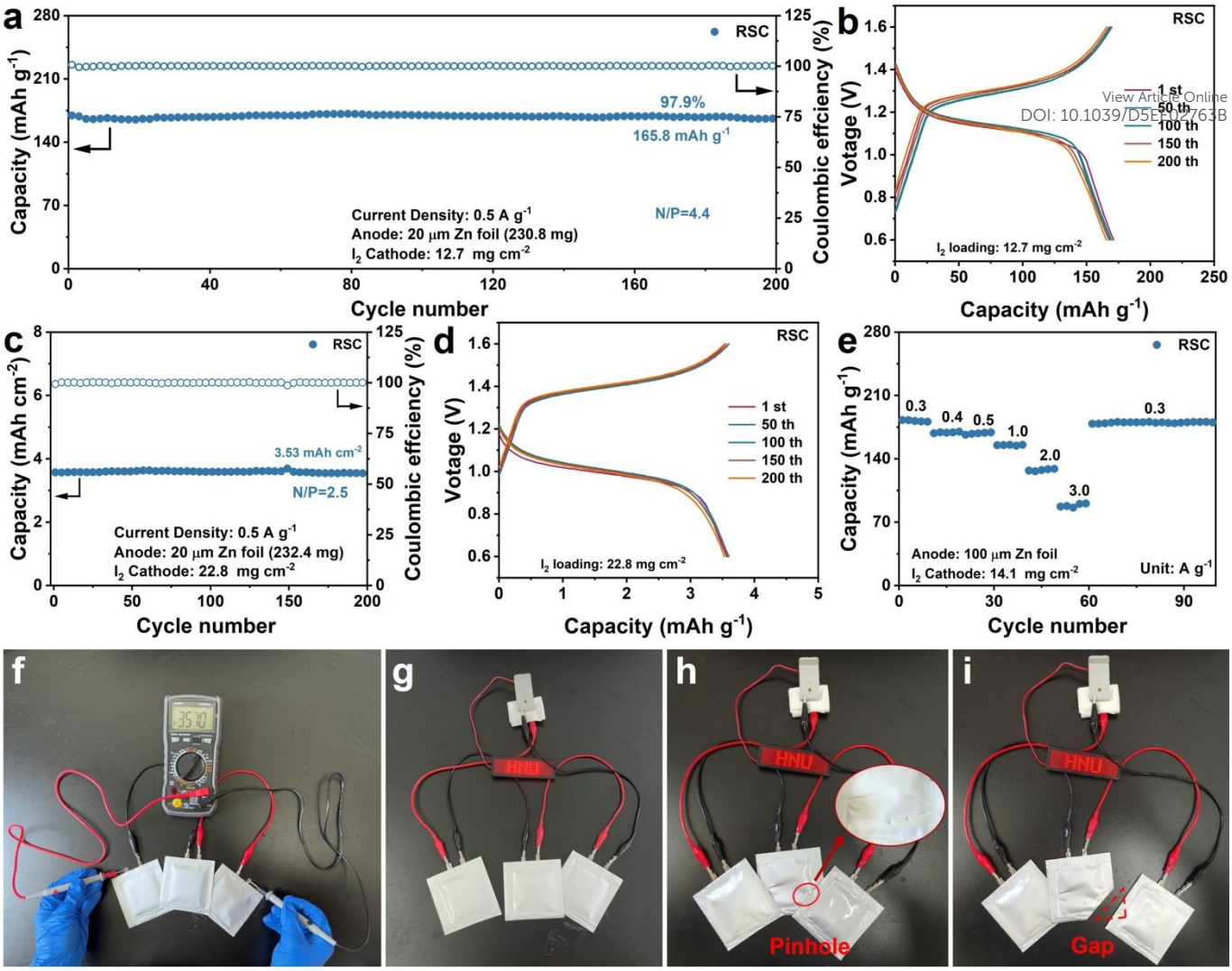

Figure 5 (a) Cycling performance and (b) the corresponding galvanostatic charge/discharge curves of Zn||AC@I_2 pouch battery in RSC electrolyte with high-iodine loading cathode of 12.7 mg cm^{-2}; (c) Cycling performance and (d) the corresponding galvanostatic charge/discharge curves of Zn||AC@I_2 pouch battery in RSC electrolyte with high-iodine loading cathode of 22.8 mg cm^{-2}; (e) Rate performance of Zn||AC@I_2 pouch battery in RSC electrolyte with high-iodine loading cathode of 14.1 mg cm^{-2}; (f) Tandem voltage test of three Zn||AC@I_2 pouch batteries; (g) Lighting up an LED panel with characters of "HNU" by Zn||AC@I_2 pouch batteries; Safety test of Zn||AC@I_2 pouch batteries in RSC electrolyte, including (h) piercing and (i) cutting states.

View Article Online
DOI: 10.1039/D5EE02763B

Data availability statement

The data that support the findings of this study are available within the manuscript and the corresponding supplementary information file.